Large Eddy Simulation of Spray Atomisation with Stochastic Modelling of Breakup

W. P. Jones[a)] and C. Lettieri

Department of Mechanical Engineering, Imperial College London,
Exhibition Road, London SW7 2AZ, UK

(Dated: 11 October 2010)

A stochastic sub-grid model for the droplet breakup in Large Eddy Simulation (LES) is developed. An Eulerian description of the continuous phase is adopted and fully coupled with a Lagrangian definition of the dispersed phase. A stochastic model is incorporated into the equation describing the evolution of the spray *pdf* in order to simulate the atomisation of sprays in the framework of uncorrelated breakup events. The results of the simulations are compared with experimental data from a diesel injector and in spray in cross flows.

Keywords: Large Eddy Simulation; Sprays; Droplet Breakup; Stochastic partial differential equations

[a)]Corresponding Author: w.jones@imperial.ac.uk

I. INTRODUCTION

The atomisation of liquid fuel plays an important role and strongly influences the combustion efficiency in many combustion related applications, such as diesel engines, gas turbines and rocket engines. Indeed, an efficient atomisation reduces the size of fuel droplets, leading to higher volumetric heat release rates, smaller evaporation times, easier light up and wider burning ranges[1]. Furthermore, the size of the droplets in the spray defines the fuel vapour distribution inside the flame and influences the exhaust concentration of pollutant emissions. A variety of models has been proposed for the liquid sprays. A statistical formulation able to describe the complex disorder encountered in sprays, including the effect of droplet growth, the formation of new droplet, collisions and aerodynamic forces was initially proposed by Williams[2]. Computational approaches to liquid sprays in turbulent flows are often based on the Lagrangian Monte Carlo procedure proposed by Dukowicz[3]. The spray is represented by discrete particles which correspond to a sample of the total population, where each computational particle represents a group of droplets possessing the same characteristics (size, velocity, composition etc.). The simplicity of implementation and the non-diffusive character of the Lagrangian approach are the main advantages of a Lagrangian compared to an Eulerian description of the spray.

Atomisation is a complex phenomena and may involve several mechanisms, determined by the initial Weber number, such as vibrational breakup, bag breakup, bag and stamen breakup, sheet stripping and catastrophic breakup. There have been several studies of liquid droplet deformation and breakup[4–8] in which attention has focused on the global behaviour of the droplets and empirical laws for the breakup process have been defined. Concerning breakup modelling, the most widely accepted mechanism is the one formulated by Reitz[9,10], where it is assumed that surfaces waves form on the liquid phase. Reitz used the wave equation of Taylor to estimate the wavelength and growth rate of the most unstable wave on the surface of the parent droplet thereby defining the conditions where the amplification of the waves would lead to the breakup of the droplets. Amongst the wave breakup models, the Taylor analogy breakup (TAB) is another important and widely accepted approach. The TAB model represents the oscillations of the parents droplets as a spring-mass system with breakup presumed to occur when the oscillations in the parent droplet exceed a critical value. Gosman and Clerides[11] proposed a variant of Reitz's approach in which the initially

unstable waves on the jet surface are assumed to be produced by turbulence in the injector nozzle.

In the context of suitable breakup models, the prediction of the representative droplet diameter (the Sauter Mean Diameter for example), and the prediction of the droplet size distribution are issues of fundamental importance. Since the 1930s several methods of modelling droplet size distributions have been proposed. A classical approach is the empirical method, based on a curve which is used to fit data collected for a wide range of atomisers and operating conditions. The curve extrapolated from the empiric data is used to characterise the distribution of droplet sizes. As reported by Lefebvre[1] typical distributions are the Rosin-Rammler, Nukiyama-Tanasawa, log-normal, root-normal and log-hyperbolic functions and a complete review of the available methods for modelling drop size distribution is provided by Babinsky[12]. As alternatives to empirical methods, several analytical approaches have been proposed. Maximum Entropy methods were developed in the late 1980s and early 1990s and have recently received attention from several investigators[13]. The Maximum Entropy method treats spray formation as a completely non-deterministic process that can be modelled using the principle of entropy maximization under the formulation of suitable constraints. On the other hand the discrete probability function (DPF) approach is an analytical method which divides the spray formation process into deterministic and non-deterministic components. The deterministic portion describes the breakup of the gross fluid structure, whilst the non-deterministic part describes the effect of fluctuating initial conditions. However, many of these models are not suited to the Large Eddy Simulation (LES) of sprays in practical applications to which the present work is directed. Recently, stochastic models inspired by the work of Mart'inez-Baz'an et al[14,15] have gained increasing popularity, due to their ability to predict the essential global features of complex spray phenomena without being computationally too expensive. A comprehensive review of some of the most relevant stochastic models for particle breakup is provided by Lasheras et al[16], where a population balance treatment for droplet breakup is formulated. The problem of closure of the breakup equation is solved by proposing models for the breakup frequency and the distribution of droplet radii. A new approach has been developed by Apte et al[17] based on a stochastic model for the breakup combined with Large Eddy Simulations of the continuous phase. The model is based on Kolmogorov's stochastic theory of the breakup of solid particles in the framework of uncorrelated breakup events (see for example Gorokhovski and

Saveliev[18]). The atomisation is represented as a random discrete process where the probability of breaking each parent particle into a given number of parts is independent of the size of the parent particle. Another related approach is that of Liu et al[19], where the implementation of the finite stochastic breakup model (FSBM) of prefilming air-blast atomisers for the secondary atomisation is proposed. In the FSBM a breakup can occur only if the size of the mother particle is larger than a critical diameter and the fragmentation generates two droplets of diameters chosen randomly with a uniform probability distribution.

In the present work, a stochastic model for the atomisation of sprays for use in combination with an LES of the gas phase is presented. The model for breakup consists of a Monte Carlo trajectory integration which reproduces the effects of the sub-grid scale motions on the droplet secondary breakup. Each breakup event is defined in a statistical manner through a Poisson release process and the evolution of the radius of the droplets is defined by a probabilistic approach. The breakup of stochastic particles is related dynamically to the flow field through the breakup frequency and the local Weber number, whilst each breakup event is defined by a life expectation procedure, governed by a Poisson distribution of characteristic frequency equal to the breakup frequency. The probability density function (*pdf*) of the number and the radius of droplets arising from the atomisation are defined in a stochastic manner. The *pdf* of particle radius resulting from a fragmentation is related to the rate of dissipation of kinetic energy and to the radius of the breaking particles. A surface energy model, based on a balance of the stresses existing at the particle surface similar to that proposed by Lasheras et al[16], has been adopted. The breakup frequency is defined by relating it to the ratio of the aerodynamic disrupting forces and the droplet surface tension. The results of the simulation are compared with experimental data from a typical diesel injection configuration and from a spray into cross flows. The Sauter Mean Diameter (*SMD*) distribution along the axis of injection in a representative diesel engine configuration is compared with the experimental data of Hiroyasu and Kadota[20] and with the DNS, RANS and LES results described by Apte et al[17] in which different breakup models are used. The results of the simulations, including *SMD* profiles, are also compared with the measurement of Park et al[21] in the spray resulting from a sequence of droplets injected transversely into a high Reynolds number jet.

II. MATHEMATICAL FORMULATION

A. Filtered Navier-Stokes equations

In LES, a spatial filter is applied to the Navier-Stokes equations. The filtering operation is defined as

$$\bar{f}(\mathbf{x},t) = \int_{\Omega} G(\mathbf{x}-\mathbf{x}';\Delta(\mathbf{x}))f(\mathbf{x}',t)d\mathbf{x}' \tag{1}$$

where G is the filter function and Δ is the filter width here assigned to be the cube root of the local cell volume,[22]. In flows where large density fluctuations occur, the introduction of density filter quantities is essential and are defined as: $\widetilde{f} = \overline{\rho f}/\bar{\rho}$.

The density weighted filtered Navier-Stokes equations, with the contribution of the dispersed phase treated as point sources of mass momentum and energy, can be written as:

$$\frac{\partial \bar{\rho}}{\partial t} + \frac{\partial(\bar{\rho}\widetilde{u_i})}{\partial x_i} = 0 \tag{2}$$

$$\frac{\partial(\bar{\rho}\widetilde{u_i})}{\partial t} + \frac{\partial(\bar{\rho}\widetilde{u_i}\widetilde{u_j})}{\partial x_j} = -\frac{\partial \bar{p}}{\partial x_i} + \frac{\partial \bar{\sigma}_{ij}}{\partial x_j} + \widetilde{\tau}_{ij} + \bar{\rho}g_i + f_i \tag{3}$$

where f_i is the force per unit mass acting on the fluid and arising from droplet drag. The Smagorinsky[23] model is used for the sub-grid scale tensor: $\tau_{ij}^d = -2\mu_{sgs}\widetilde{S}_{ij}$, where τ_{ij}^d is the deviatoric *sgs* stress with $\mu_{sgs} = \bar{\rho}\left(C_s\Delta^2\right)||\widetilde{S}_{ij}||$. C_s is the Smagorinsky constant equal to 0.07 and $||\widetilde{S}_{ij}||$ is the Frobenius norm $||\widetilde{S}_{ij}|| = \sqrt{2\widetilde{S}_{ij}\widetilde{S}_{ij}}$ of the filtered strain tensor, $\widetilde{S}_{ij} = 0.5\left(\frac{\partial \widetilde{U}_i}{\partial x_j} + \frac{\partial \widetilde{U}_j}{\partial x_i}\right)$. Dynamic versions of the Smagorinsky model[24,25] allow the value of the parameter C_s to be determined as a function of time and position. However, there is little to be gained by the use of more complex *sgs* models in the case of high Reynold number free flows of the type considered. As is clear from the results presented below the standard Smagorinsky model gives good results.

B. PDF modelling of sprays

Following Bini and Jones[26] a probabilistic description of the spray is adopted with the state of the spray being characterised uniquely in terms of the droplet radius, r the droplet velocity, v the droplet temperature, θ and number, n. The required joint *pdf* is $\overline{\mathrm{P}}_{spr}(\mathbf{V},\mathrm{R},\Theta,\mathrm{N};\mathbf{x},t)$, where $\{\mathbf{V},\mathrm{R},\Theta,\mathrm{N}\}$ is the 'phase' space for $\{\mathbf{v},\mathrm{r},\theta,\mathrm{n}\}$, which can be

obtained, after suitable modelling, from:

$$\frac{\partial \overline{\mathrm{P}}_{spr}}{\partial t} + \nabla_{\mathbf{v}} \cdot \left(\mathbf{a}\overline{\mathrm{P}}_{spr}\right) + \frac{\partial\left(\dot{\mathcal{R}}\overline{\mathrm{P}}_{spr}\right)}{\partial R} + \frac{\partial\left(\dot{\mathcal{T}}\overline{\mathrm{P}}_{spr}\right)}{\partial \Theta} + \frac{\partial\left(\dot{\mathcal{N}}\overline{\mathrm{P}}_{spr}\right)}{\partial N} = 0 \tag{4}$$

where $\mathbf{a}, \dot{\mathcal{R}}, \dot{\mathcal{T}}$ and $\dot{\mathcal{N}}$ represent:

$$\mathrm{E}\left(\frac{\mathrm{D}\psi_k}{\mathrm{D}t}\middle|\, \mathbf{\Psi} = \mathbf{\Phi}\right) \text{ where } \mathbf{\Phi} = \mathbf{v}, \mathrm{r}, \theta \text{ and } \mathrm{n}$$

and $\mathrm{E}\left(\frac{\mathrm{D}\psi_k}{\mathrm{D}t}\middle|\, \mathbf{\Psi} = \mathbf{\Phi}\right)$ is the expect value of $\frac{\mathrm{D}\psi_k}{\mathrm{D}t}$ conditioned upon $\mathbf{\Psi} = \mathbf{\Phi}$ anywhere in the filter volume. These quantities are unknown and models are required.

In order to first model and then solve equation (4) it is replaced with an equivalent system[27] of stochastic ordinary differential equations describing the trajectories of stochastic particles in the phase space $\{\mathbf{V}, \mathrm{R}, \Theta, \mathrm{N}\}$. The models for dispersion and evaporation of droplets have been extensively described in previous publications[28,29] and are here only briefly outlined. In the present case only models for the conditional Lagrangian rate of change of the droplet velocity and droplet number are required; there is no evaporation so that models are needed only for droplet dispersion and droplet breakup.

1. Droplet Dispersion

The Ito equivalent of the closed form of equation (4) that describes the evolution of the spray *pdf* in space and time is given by the following system of equations:

$$\begin{aligned} d\mathbf{x}_p &= \mathbf{v}_p dt \\ d\mathbf{v}_p &= \mathbf{a}_p dt \end{aligned} \tag{5}$$

where the subscript p represents the p^{th} particle. Consistent with this the motion of a stochastic particle in a turbulent flow field can be viewed as a random process with position determined by a deterministic part, evaluated in terms of filtered values and a stochastic component arising from the *sgs* turbulent motions of the gas phase. In this study only viscous drag and gravitational forces are considered and a stochastic Markov model[26,30] is used to represent the influence of the unresolved carrier gas velocity fluctuations experienced by a stochastic particle p over a time dt which is added to the deterministic contribution:

$$d\mathbf{v}_p = \tau_p^{-1}\left(\widetilde{\mathbf{U}}_p\left(t\right) - \mathbf{v}_p\right)dt + \frac{\rho_\ell - \bar{\rho}_p}{\rho_\ell}\mathbf{g}dt + \left(C_o\frac{k_{sgs}}{\tau_t}\right)^{1/2} d\mathbf{W}_t \tag{6}$$

where ρ_ℓ is the particle density, $\mathbf{v}_p$ is the velocity of the p^{th} particle, $\bar{\rho}_p$ and $\widetilde{\mathbf{U}}_p$ are the filtered gas density and velocity at the particle position, k_{sgs} is the unresolved kinetic energy of the gas phase, C_o is a model constant, $d\mathbf{W}_t$ represents the increment of the Wiener process and $\mathbf{g}$ is the gravitational acceleration. τ_t is a sub-grid timescale, which determines the rate of interaction between the particle and turbulence dynamics, defined as:

$$\tau_t = \tau_p \left(\frac{\tau_p}{\frac{\Delta}{\sqrt{k_{sgs}}}} \right)^{0.6} \tag{7}$$

This definition of time scale has been demonstrated[30]to reproduce the heavy tailed pdfs observed experimentally. The particle relaxation time, τ_p is given by: $\tau_p^{-1} = \frac{3}{8}\frac{\rho_f C_D}{\rho_p R}|\widetilde{\mathbf{U}}_p - \mathbf{v}_p|$, where the drag coefficient C_D is obtained from Yuen and Chen[31]:

$$C_D = \begin{cases} \frac{24}{Re}\left(1 + \frac{Re^{2/3}}{6}\right) & : \quad 0 < Re < 1000 \\ 0.424 & : \quad Re \geqslant 1000 \end{cases} \tag{8}$$

where Re is the Reynolds number based on the droplet diameter and the relative velocity of the droplet with respect to the gas phase.

The drag coefficient, equation (8) was developed for spherical shape particles and is appropriate as long as the droplet remains close to this shape. However in some of the cases to be considered the deformation effects are so large that the use of equation (8) is no longer justified. In particular the droplets can deform into a balloon or parachute-like shapes and the drag coefficient should be adjusted accordingly. In Volgin and Yugai[32] and Stekol'shchikov et al[33] and references therein, the drag coefficients of single significantly deformed droplets were measured as a function of Weber number, We. The major result was that C_D increases with We up to a value of about 2 for $We \geq 50$. The drag force also depends on the orientation of the droplet and the flow and strictly it cannot be expressed in terms of a scalar drag coefficient. The extension of equation (6) to account for variable droplet shapes is a complex and difficult task and is not entirely consistent with the assumption of particles acting as point forces and sources. For this reason a scalar drag coefficient is retained. Some justification for this is provided by the statistical approach adopted: in a population of many droplets experiencing the same conditions the modified C_D will apply on average in all directions, at least if the turbulence is approximately isotropic. The corrected

drag coefficient[34] is thus as follows:

$$\bar{C}_D = \begin{cases} C_D & : \quad We \leq We_c \\ C_D + \left(\frac{We - We_c}{50 - We_c}\right)(2 - C_D) & : \quad We \leq 50 \\ 2.0 & : \quad We > 50 \end{cases} \tag{9}$$

where the Weber number is defined as $We = \dfrac{2\rho_g r_p |\tilde{\mathbf{U}}_p - \mathbf{v}_p|^2}{\sigma}$ and where σ is the surface tension of the dispersed phase. $We_c = 12$ is the critical value of Weber number below which breakup does not occur. The results of a computational study[35] have demonstrated that internal flow within droplets and non-sphericity can both have an important influence on drag. Based on these results a correlation was developed for predicting the drop shape as a function of the dimensionless parameters governing the system. An extended drag model for deforming liquid drops was also proposed. However, the main focus of the present paper is droplet breakup and the simple modification, equation (9 was considered sufficient. The *sgs* kinetic energy is obtained from $k_{sgs} = \left(2\Delta\nu_{sgs}\tilde{S}_{ij}\tilde{S}_{ij}\right)^{\frac{2}{3}}$, an expression derived using equilibrium arguments.

2. Droplet Breakup

The conditional Lagrangian rate of change of particle number, $\dot{\mathcal{N}}$ is used to represent droplet breakup processes. Each stochastic particle contains a given number of droplets, n that represent the probable number of particles with radius in the range $r < r' < r + dr$, located within the spatial position $\mathbf{x} < \mathbf{x}' < \mathbf{x} + d\mathbf{x}$ and with a velocity $\mathbf{v} < \mathbf{v}' < \mathbf{v} + d\mathbf{v}$ at time t. In the present work the variation in the number n arises only through droplet nucleation, coalescence and breakup. There have been numerous studies of the dynamics of particles in dispersed flow systems and much of this work can grouped under the heading *population balance equation (PBE) models*[36,37]; a recent and comprehensive review is provided by Rigopoulos[38]. Examples of applications of the PBE to droplet breakup include the works of Williams[2], Lasheras et al[16] and Mart'inez-Baz'an et al[14,15].

The present model for breakup involves a Monte Carlo trajectory integration which reproduces the effects of the *sgs* motions on the secondary breakup of droplets. Each breakup event is defined in a statistical manner through a Poisson release process and the evolution of the radius of the droplets is defined in a probabilistic manner. The breakup of stochastic

particles is related dynamically to the flow field through the breakup frequency and the local Weber number. The rate of change of the number of droplets in a stochastic particle, $\dot{\mathcal{N}}$ is equal to the rate of change of the number of particles due to breakup. The latter can be expressed[16] as the sum of the birth rate of particles of size r resulting from the breakup of larger ones, and the death rate of particles of size r due to their breakup into smaller ones:

$$\dot{\mathcal{N}} = \int_r^\infty q(r_0) f(r, r_0) \omega(r_0, We) n(r_0) dr_0 - \omega(r, We) n(r) \tag{10}$$

where $\omega(r, We)$ is the breakup frequency of particles of size r; $q(r_0)$ is the mean number of particles resulting from the break up of a mother particle of size r_0; $f(r, r_0)$ is the size distribution of daughter particles formed from the breakage of a mother particle of size r_0. In order to close equation (10), a suitable model for the breakup frequency $\omega(r)$, the expected number of daughter particles $q(r)$ and the *pdf* of daughter particles $f(r, r_0)$ must be defined. In the present work the following expression for the breakup frequency is adopted:

$$\omega(r_p, We) = 0.5 C_b \sqrt{\frac{\rho_g}{\rho_\ell}} \frac{|\tilde{\mathbf{u}} - \mathbf{v}_p|}{r_p} + K_g \frac{\sqrt{\beta(\epsilon 2r_p)^{2/3} - 12\sigma/\rho_g r}}{2r_p} \tag{11}$$

The first term on the right hand side of equation (11), with $C_b = \sqrt{1/3}$, is the '*deterministic component*' of the breakup frequency, defined according to O'Rourke and Amsden[39] and Faeth et al[40] and is dynamically related to the local flow properties through the velocity and density of the gas phase. The second term, where ϵ is the rate of dissipation of kinetic energy obtained from $\epsilon = 2(\nu + \nu_{sgs})\tilde{S}_{ij}\tilde{S}_{ij}$, represents the *sgs* contribution and is based on a work of Mart'inez-Baz'an at al[14,15] who studied the break up of air bubbles in a stirred vessel. In this case the dispersed phase is transported by the continuous phase with no relative velocity between bubbles and water; hence fragmentation is due only to turbulent velocity fluctuation. Mart'inez-Baz'an at al consider a gaseous dispersed phase and a liquid continuous phase whereas in this work we are concerned with liquid droplets in a gas continuous phase. However, the formulation of Mart'inez-Baz'an at al is also applied in the present gaseous continuous phase-liquid dispersed phase case with the values of the empirical constants being retained at $K_g = 0.25$ and $\beta = 8.2$. In equation (11) the *sgs* component to the breakup frequency is defined by relating it to the ratio of the aerodynamic

disruptive forces acting on a droplet and the stabilizing surface forces, characterised by the surface tension of the liquid. This is achieved by relating the breakup frequency to the ratio of the droplet diameter and a breakup velocity. This breakup velocity is presumed to be proportional to the difference between the surface pressure forces arising from turbulent fluctuations of the continuous phase and the restoring forces associated with surface tension. The initial size of the droplets is presumed such that it lies within the inertial subrange so that the velocity is then proportional to the droplet diameter and the turbulence energy dissipation rate. The average number of particles formed from the breakup at time t is frequently known and following Ramkrishna[36] it is assigned the value 2.

Historically there have been three predominant approaches[12,13,16] to the modelling of $f(r, r_0)$. These are statistical models, phenomenological models based on the change in surface energy of a breaking particle and hybrid models, which are based on a combination of both. In the present work a surface energy model, based on a stress balance, has been adopted. When a mother particle breaks, $q(r)$ daughter stochastic particles with characteristic radii r_1 and r_2 are generated. The number of breaking droplets inside the mother stochastic particle is equally distributed into the two newly added stochastic particles. Following the work of Lasheras et al[16] the probability of the formation of two daughter particles of size r_1 and r_2 is presumed proportional to the product of the differences between the two excess forces. The corresponding probability density function used to determine the radii r_1 and r_2 is:

$$f^*(r^*) = \frac{[r^{*2/3} - \Lambda^{5/3}][(1 - r^{*3})^{2/9} - \Lambda^{5/3}]}{\int_{r^*_{min}}^{r^*_{max}} [r^{*2/3} - \Lambda^{5/3}][(1 - r^{*3})^{2/9} - \Lambda^{5/3}]dr} \tag{12}$$

where $r^* = r_1/r_0$, $\Lambda = r_c/r_0 = (r_{min}/r_0)^{2/5}$, $r_{min} = 0.5(12\sigma/(\rho\beta 2r_0))^{3/2}\epsilon^{-1}$ and $r_c = 0.5(12\sigma/(\beta\rho))^{3/5}\epsilon^{-2/5}$. The radii r_1 and r_2 are related by conservation of mass:

$$r_2 = r_0\left[1 - \left(\frac{r_1}{r_0}\right)^3\right]^{1/3} \tag{13}$$

as are the radii r_{max} and r_{min}. The method adopted to generate random radii consistent with the given probability distribution function is Inverse transform sampling.

The treatment of droplet breakup from a trajectory point of view, using equation (4), requires additional modelling in order for it to be computationally feasible. When a trajectory point of view is adopted and the breakup of droplets occurs, the daughter particles produced should a priori follow their own new independent trajectories in phase space. If the break up

is modelled as a continuous process, new trajectories, representing the emission of daughter particles, should be released continuously from the mother trajectory. The computational load of such task would be very high and for this reason a discrete Poisson release process is used.

The probable number of droplets in a stochastic particle which are likely to experience fragmentation is computed each time step as specified by the second term of the right hand side of equation (10). However, the stochastic particles are presumed not to break continuously. Instead, the global number of droplets that are broken at every instant is stored as: $N^{broken} = \int_{t_0}^{t} \omega(r) N_t dt$, where t_0 and t are respectively the time of birth of the particle and the time of fragmentation, while N_t is the number of droplets at the instant t. A mother stochastic particle with characteristic radius r_0 is presumed to fragment if its age is larger than its expected life, defined by a Poisson distribution with characteristic frequency equal to the breakup frequency. The Lagrangian rate of change of the number of droplets represented by a stochastic particle due to the Poisson release process can be expressed as:

$$\delta N_t = -N^{broken} \delta C_t$$

and δC_t is zero if the age of the particle is smaller than the expected life and one otherwise. The expected life is computed[34] as the random variable $pdf(T_{split} = t) = \omega(r) e^{-\omega(r)t}$.

The probable number of the stochastic particle due to droplets of radius $r^* > r$ which break exactly into a droplet of radius r (the so called '*rate of birth*' of equation (10)) is added to $n(r, t)$ by merging the stochastic particle with other newly formed stochastic particles at approximately the same position and with the same dimensions. The number of actual droplets represented by a single stochastic particles is restricted to be less than a finite number, N_{pmax}. If a breakup occurrence generates a number of droplets larger than N_{pmax} then the resulting stochastic particle is cloned and replaced by two stochastic particles with identical properties, each with $n \leq N_{pmax}$. In the present work N_{pmax} is set to 10.

The presented model serves to reduce the computational cost of the simulation, with respect to the breakup model. However this comes at a cost. Whilst the Poisson release process, along with the stochastic particle treatment, reduces the overall computational cost of the simulation, the discontinuous stochastic nature of the model can result in it being slow to converge and longer run times may often be required to give a reliable averaged solution.

The present LES droplet breakup formulation has some similarities to the model of Apte et al[17] and Gorokhovski and Saveliev[18] though there are important differences. In their population balance formulation an expression for the breakup frequency similar to the deterministic breakup component of the present paper, equation (11) is used and the critical value of droplet size for breakup is determined in terms of an estimated rms of the relative droplet-to-gas velocity. Probably the major difference which sets the present model apart is the different way of computing the diameter of the daughter particles. In contrast to the current approach the diameter of the newly formed droplets is found according to a diameter distribution which evolves in time from an initial distribution. A Fokker-Plank equation of the diameter distribution is formulated and linked to the flow-field properties through the breakup frequency and the Weber number. In the present work a diameter distribution is computed for each droplet independently depending on the droplet diameter, the gas phase velocity and kinetic energy dissipation rate. The diameter of the daughter particles is computed according to this distribution.

III. RESULTS AND DISCUSSION

The particle breakup model described above is combined with a conventional LES to simulate the droplet characteristics in two configurations.

A. Diesel Spray in Stagnant Flow

The first of these corresponds to the experimental diesel injector study of Hiroyasu and Kadota[20] where diesel fuel is injected into a closed cylinder, of length 138 mm and diameter 56 mm, containing pressurised nitrogen at ambient temperature. The injector comprises a single hole nozzle. Since the chamber temperature is low, evaporation of the liquid fuel is negligible, allowing the study of droplet breakup alone. In the simulations large droplets of diameter 300 μm corresponding to the nozzle diameter are injected and the time step is held constant at 1.5 μs. Initially, the nitrogen is quiescent but recirculation zones eventually arise through momentum transfer from the liquid jet to the gas-phase. A single case with pressure 1.1 MPa is simulated. The mass flow rate of the liquid is obtained from the injection velocity, nozzle diameter and the time of injection. The diesel fuel density is $840 Kg/m^3$, the

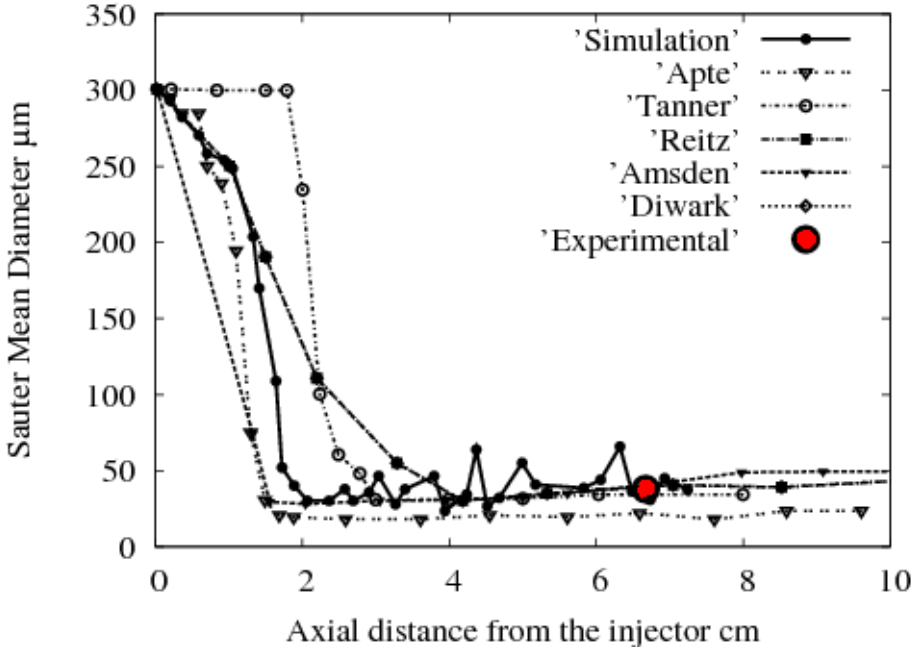

FIG. 1. Sauter Mean Diameter distribution along the axis of injection - Distance in cm from the injector (x axis) SMD in μm (y axis)

surface tension is 29.5 mN/m, the gas pressure is 1.1 MPa and the density of the gas phase is thus $13.57 kg/m^3$. The viscosity of nitrogen is 1.77×10^{-5} Kg/ms and its temperature is 20 C. As a consequence droplets are injected with a velocity of 102 m/s in the z-direction and at a position corresponding to $x = 0$, $y = 0$ and $z = 0.0002$ m. For the simulations a cylindrical domain of length 138 mm and diameter 56 mm and a uniform grid comprising $65 \times 65 \times 100$ nodes was used.

The results of the simulations are presented in Figures (1-3). The variation of the Sauter Mean Diameter of the droplets along the axis of injection are compared in Figure (1) with experimental data and the predicted results quoted by Apte et al[17] who present the results of several breakup models. As is evident the results of the present simulation are in good agreement with the measurement. The simulated spray penetration, displayed in Figure (2), is also in very close agreement with the measured data. Figure 3 shows an instantaneous snapshot of the spray with both the droplets and the flow field of the continuous phase being displayed. The flow and turbulence of the nitrogen is induced by the coupling of the liquid phase with the gas phase. The resulting jet structure effects the droplets dispersion and

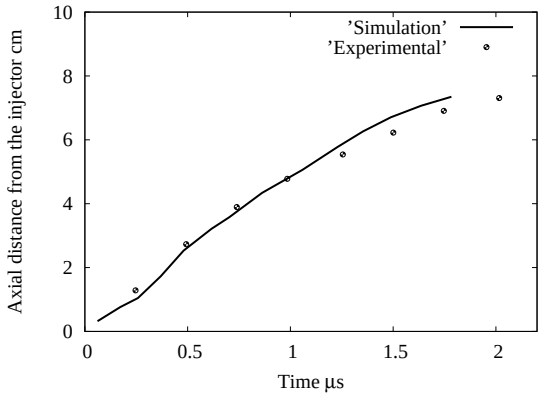

FIG. 2. Spray penetration, time in μs, distance in cm

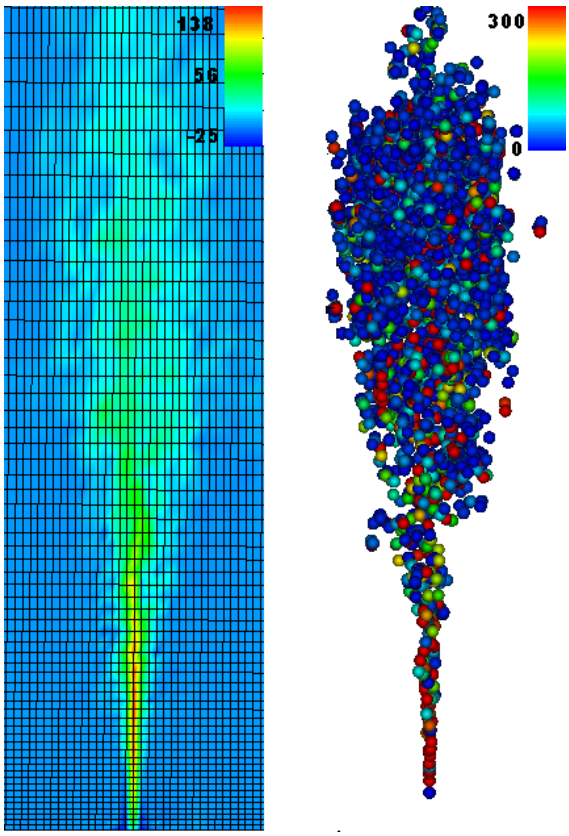

FIG. 3. Snapshot of droplets

atomisation.

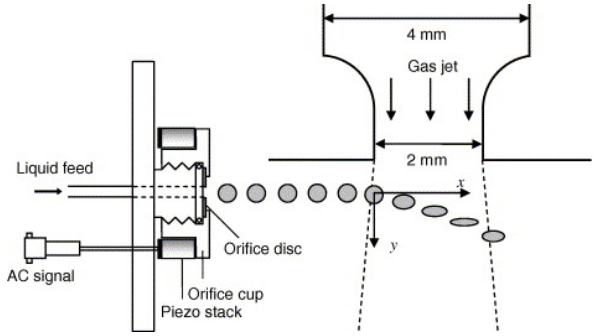

FIG. 4. Schematic diagram of the experimental droplet generator and gas nozzle

B. Diesel spray in cross flow

The second case to be considered corresponds to the experimental investigation of Park et al[21] in which a sequences of diesel droplets are injected at right angles to a high Reynolds number air jet. A schematic diagram of the test case is presented in Figure (4). The droplets are generated by a vibrating orifice injector which results in droplets of approximately uniform size (around 180 μm) being injected at a velocity of 13.4 m/s. The air jet emanates from a nozzle of inner diameter 2 mm and the injector is located 1.5 mm downstream of the nozzle exit. Because of the contoured nature and dimensions of the nozzle, the boundary-layer effects are minimised, ensuring that the thickness of the shear layer to be penetrated by the droplets at the edge of the jet is as thin as possible. The droplets traverse the air jet and consequently disintegrate and are deflected. The atomisation results in a variety of different diameter droplets. As can be seen in Figure (5), the measurement points are located at intervals of 2mm in both the axial and radial directions, within the range in which the breakup actively occurs. The Weber number is an important parameter which indicates the potential for droplet breakup, with breakup occurring above a critical value. Consequently three different breakup regimes, obtained by varying the air jet velocity, were investigated. A multiblock o-grid of $70 \times 70 \times 220$ nodes was used for the computations. The mesh was locally refined near the air jet inlet and the cell sizes were between 200 and 300 μm in the region around the liquid injection point.

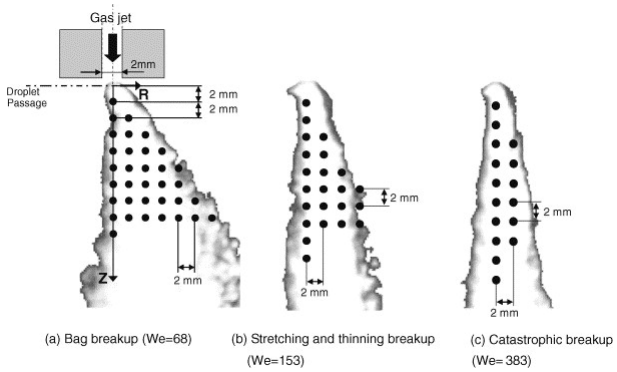

FIG. 5. Experimental Study: measurement locations

1. Bag breakup regime (We=68)

The first regime considered corresponds to a Weber number, We=68 . When the Weber number is slightly higher than the critical value, a thin hollow bag originates at the droplet stagnation point. The bag grows and bursts forming a number of small and large fragments[1]. Some large fragments are able to cross the jet intact and experience further fragmentation in the quiescent flow area, where the Weber numbers are much smaller. In contrast small fragments with low momentum are captured by the jet and are transported by the turbulent eddy structure of the fast moving air jet. The stochastic Markov dispersion model, equation (6) exerts a dominant influence on the results to be presented and this is illustrated clearly in Figures (6) and (7) which show simulations with and without the stochastic dispersion term included. Figure (8) shows a comparison between the global experimental and simulated

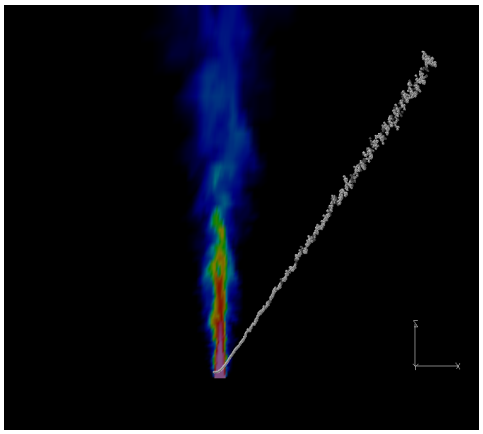

FIG. 6. Simulation without stochastic term for droplets dispersion

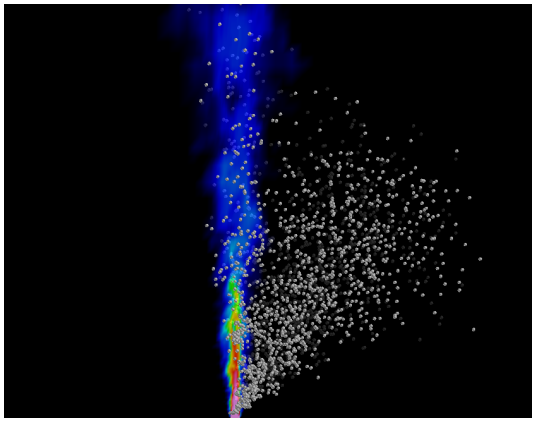

FIG. 7. Simulation with stochastic term for droplets dispersion

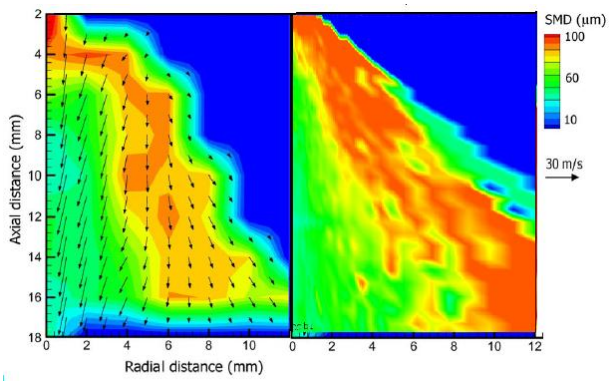

FIG. 8. Sauter Mean Diameter of droplets: left experiments, right simulations

contours of *SMD*: the results of the simulations are in good overall agreement with the measurements. In the bottom right region, some over prediction of the simulated *SMD* compared to the experiments is evident, although the practical significance of this may not be important in cases where evaporation and/or combustion arise.

Figure 9 shows the general behaviour of the experiments compared with the simulations whereby it is evident that the global features of the system are well captured. Small droplets(red) and large droplets (blue) follow different trajectories, consistent with their differing momentum and the experimental data. The simulated radial profiles of *SMD* are compared with the experimental data at an axial distance of 8, 12 and 16 mm in Figures 10 to 12. The results of the simulation and measurements are again in reasonable accord. The simulations appear to reproduce the measured droplets sizes to a good accuracy. In

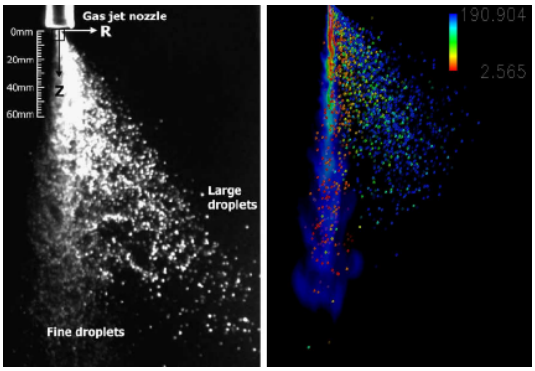

FIG. 9. Sauter Mean Diameter of droplets: left experiments, right simulations

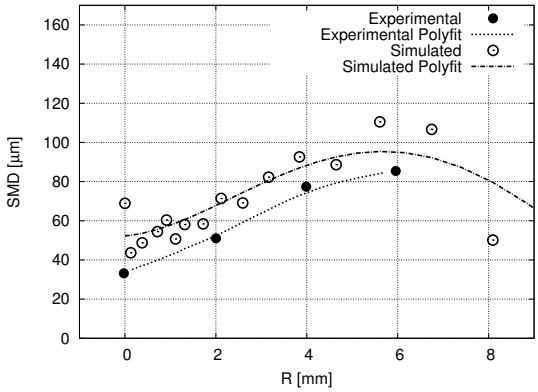

FIG. 10. Radial Profile of *SMD* at a distance of 8 mm from the jet nozzle. Distance in mm (x axis) *SMD* in μm (y axis)

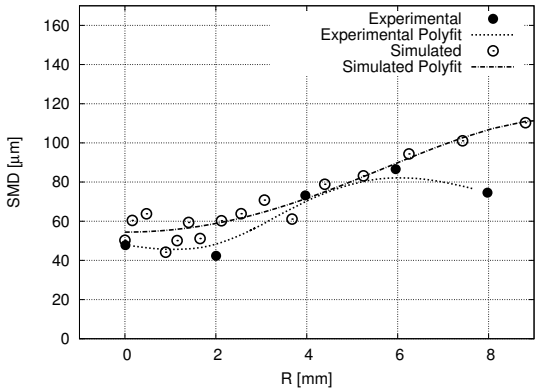

FIG. 11. Radial Profile of *SMD* at a distance of 12 mm from the jet nozzle. Distance in mm (x axis) *SMD* in μm (y axis)

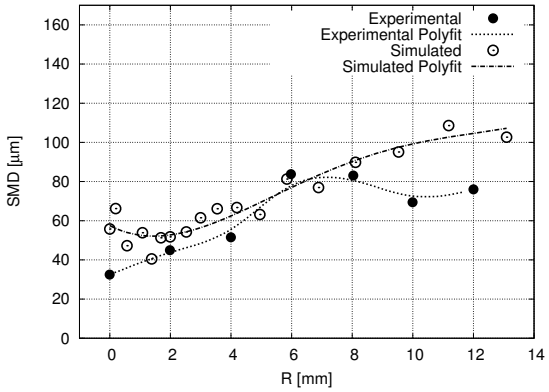

FIG. 12. Radial Profile of *SMD* at a distance of 16 mm from the jet nozzle. Distance in mm (x axis) *SMD* in μm (y axis)

the case of the profiles at 12 and 16 mm downstream there is an indication of the same over prediction of droplet *SMD* in the outer part of the jet, $r > 7$ mm, corresponding to a region of very low gas velocity, that is evident in the contour plot of Figure 8. The maximum discrepancy is around 20 μm

The axial mean velocity of the droplets is compared with experimental data at the same locations in Figures 13 to 15. The simulated radial profile of droplet velocity at $z = 8$ mm can be seen to be excellent agreement with the measurements. At $z = 12$ mm the measured and simulated centreline velocities are in close agreement though in the outer part of the jet the velocities are over predicted by around 5 m/s. At the furthermost downstream location, Figure 15 the simulated velocities are everywhere larger than the measured values by around 7 m/s though the shapes and widths of the two profiles are closely similar. This discrepancy may well be associated with the relatively crude method adopted, equation (9) to account for the drag of what are essentially non-spherical droplets in this regime.

The *pdfs* of droplet diameter at the injection point (z=0, r=0) and at the downstream location (z=8mm, r=6mm) are shown in Figures 16 to 19. As is evident, Figures 16 and 17, the constructed *pdf* at the injection point is consistent with the experimentally measured distribution. The comparison of measured and simulated *pdfs* at the downstream location, Figures 18 and 19, indicate that the model is capable of reproducing the measured behaviour to a good accuracy. There is some small discrepancies at large droplet sizes (greater than around 100 μm) and, in contrast to the experiments a finite but small probability of observing

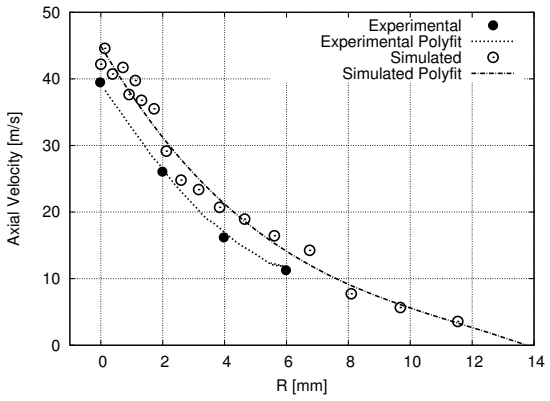

FIG. 13. Radial profile of droplet mean axial velocity at a distance of 8 mm from the jet nozzle.

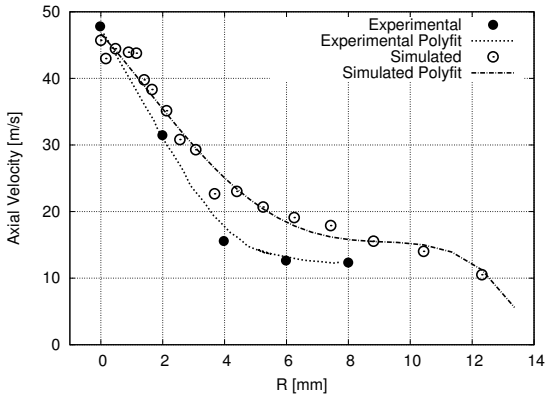

FIG. 14. Radial profile of droplet mean axial velocity at a distance of 12 mm from the jet nozzle.

large droplets of diameter 180 μm is predicted. In other respects the level of agreement achieved is good.

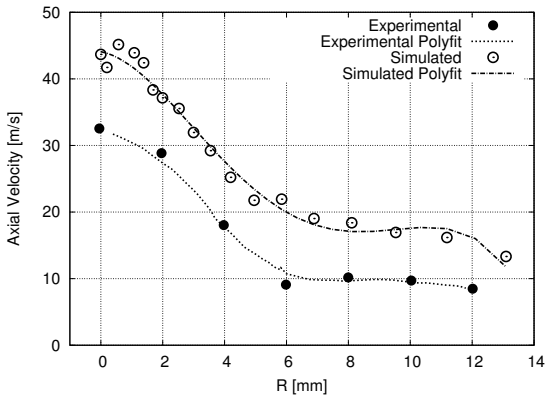

FIG. 15. Radial profile of droplet mean axial velocity at a distance of 16 mm from the jet nozzle.

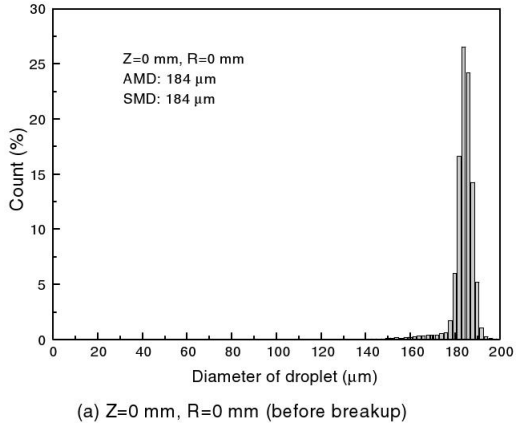

(a) Z=0 mm, R=0 mm (before breakup)

FIG. 16. Measured probability density function of droplet diameter at injection

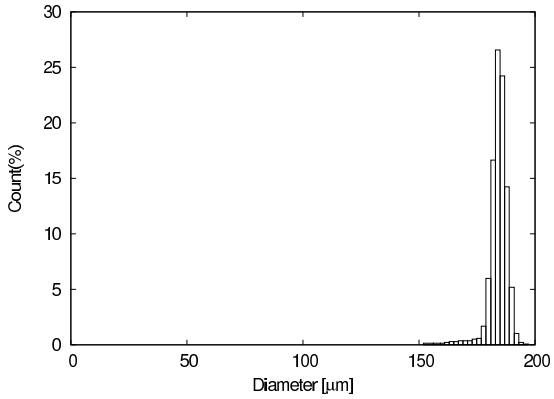

FIG. 17. Simulated probability density function of droplet diameter at injection

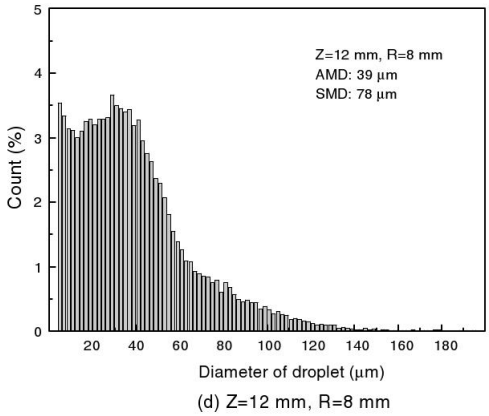

FIG. 18. Measured probability density function of droplet diameter at $z = 12$ mm , $r = 8$ mm

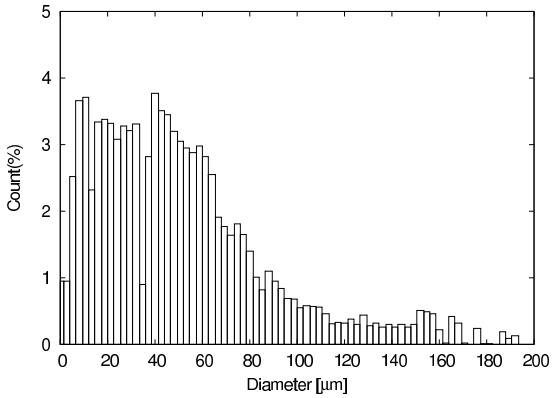

FIG. 19. Simulated probability density function of droplet diameter at $z = 12$ mm , $r = 8$ mm

2. *Stretching and thinning breakup regime (We=153)*

In the stretching and thinning breakup regime, droplets are observed to disintegrate[21] at their edge because of a 'suction' stress toward the flow direction generated at the surface of the droplet. In this case, a shearing action due to the high-speed gas flow on the droplet causes the deformation and separation, leading to the formation of smaller fragments - compared to the bag breakup regime. The measured and simulated axial profiles of droplet

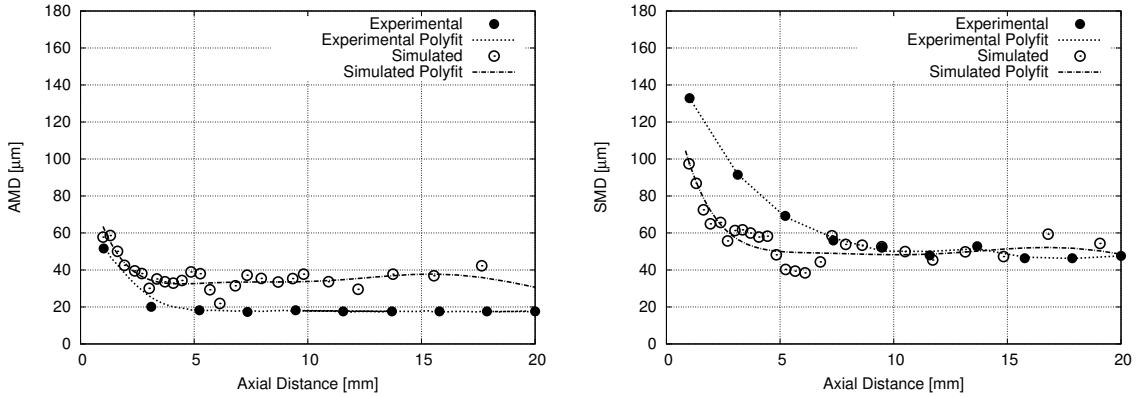

FIG. 20. Axial profiles of mean droplet diameter AMD and SMD along the centreline (We=153).

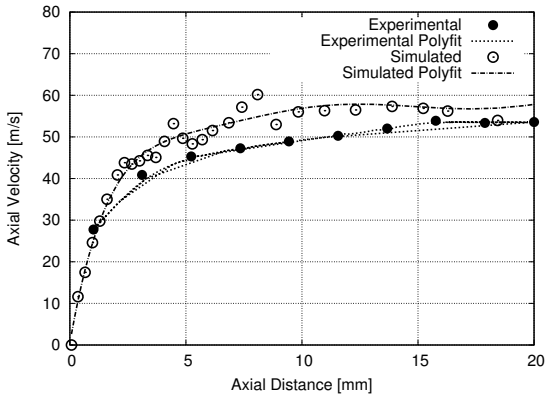

FIG. 21. Axial profile of mean droplet velocity along the centreline (We=153).

AMD and SMD along the jet centreline are compared in Figure 20. The droplet diameter falls from 184 μm at the injector to an $AMD \approx 60\mu$m and a $SMD \approx 135\mu$m at $z = 1$mm. The measured and simulated AMD profiles are in reasonable accord for $z < 3$mm but further downstream the mean diameters are approximately constant with a simulated value

of around 40μm compared with a measured value of about 20μm. On the other hand the simulated *SMD* is under predicted by around 20μm for $z \lesssim 5\mu$m but beyond $z \geq 6\mu$m the measured and simulated profiles are in close agreement. The simulated and measured variations of droplet mean axial velocity along the centreline are compared in Figures 21. Reasonably good agreement is displayed with a slightly higher velocities evident, by around 5m/s, in the simulations for $z > 6$mm.

3. Stretching and thinning breakup regime (We=383)

As the Weber further increases, the breakup regime changes to the catastrophic breakup. The breakup of the droplet occurs suddenly due to the wave instability on the droplet surface. The diameters of the daughter droplets are smaller than in the previous regimes as the droplets appears to disintegrate almost immediately generating a large number of very small fragments. For this reason the drag law, equation (8) was applied rather than the modified version, equation (9). In this case only the profile of droplet *AMD* along the centreline is available with the simulated and measured profiles being shown in Figure 22. The measured *AMD* falls from 184μm at the injector to approximately 20μm at $z = 1$mm on the jet centreline while the simulated value at this location is around 40μm. However for $z \geq 3$mm the simulated and measured profiles are in excellent accord. The simulated and measured variations of droplet mean axial velocity along the centreline are compared in Figure 23. The two profiles are in qualitative agreement with the simulated velocities being somewhat higher than measured values. The comparison of the simulated values

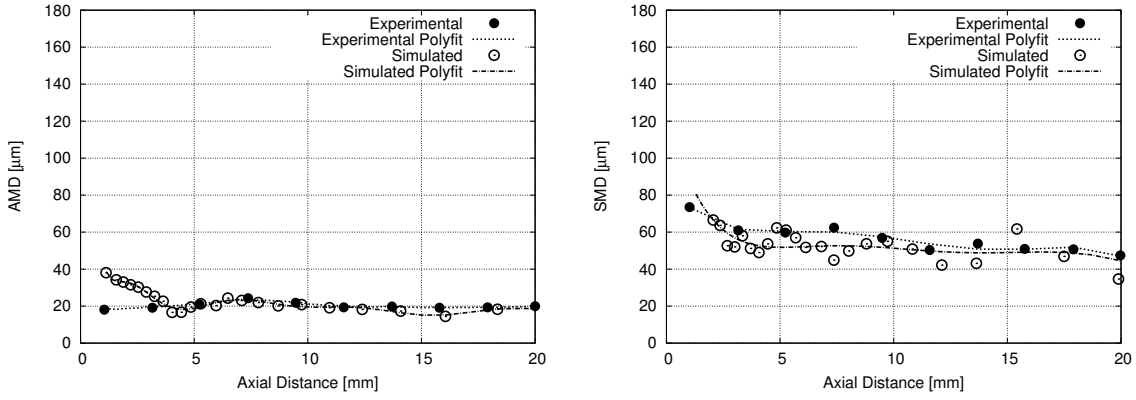

FIG. 22. Axial profile of mean droplet diameter (*AMD*) and *SMD* along the centreline (We=383).

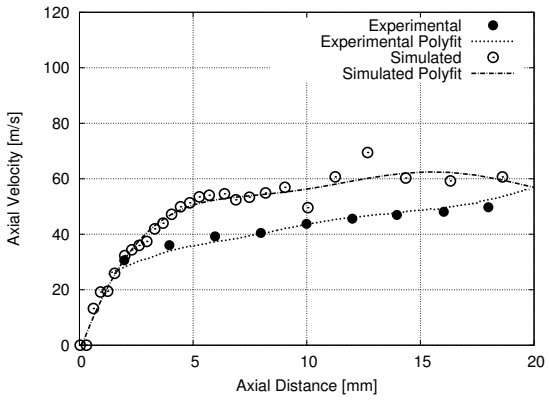

FIG. 23. Axial profile of droplet mean velocity along the centreline (We=383).

with the experimental ones shows an underestimation of the mean diameter (about 10 μm) and a substantial over prediction of the mean velocity. The reasons for this are unclear but they may be associated with limitations associated with quasi-spherical droplet assumptions implied by the droplet drag law used.

IV. CONCLUSIONS

An LES probabilistic approach for droplet secondary breakup has been formulated and validated. Overall the formulation was found to yield good agreement with experimental data. The predicted droplet *SMD*s were compared with two test cases: a single cycle of a diesel fuel injector issuing droplets into quiescent pressurised nitrogen and mono-dispersed droplets injected into a cross flow. In the former case the size of the droplets and the spray penetration show a reasonably good agreement with the measurements and with the results of other authors using different models. The global behaviour of the system is well captured, and the droplets appear to breakup, generating a constellation of fragments with diameters in agreement with the measured data. For the case of droplets injected into a cross flow a range of Weber numbers are encountered. It is found that the model is able to generate droplet fragments with different sizes as well as reproducing the global features of the experiment. The simulations indicate that large droplets with high momentum cross the jet whilst small droplets do not. They are captured and transported by the turbulent eddying structures thus reproducing the observed *SMD* distribution. The simulation showed predicted *SMD*s in good local and general with measurements. The analysis of different breakup

regimes with different Weber number has demonstrated that the model is able to adapt to different breakup mechanism. As the relative velocity between the gas and the liquid phase increases, the Weber number increases and the droplets break up displaying completely different physical regimes. The formulation is based on a presumption of spherical droplets and in some of the cases considered the deformation is such that droplets can deform into a balloon or parachute-like shapes. In these circumstances the drag force depends both on the droplet shape and its orientation with respect to the flow. A simple modification to the drag coefficient is proposed in an attempt to account for such effects though strictly a much more detailed and complex treatment is required. The limitations associated with the use of a modified quasi-spherical drag law under such conditions may, however be ameliorated by the statistical nature of the model. It appears capable of reproducing the global behaviour to a good accuracy, though some of the discrepancies that do arise are undoubtedly associated with limitations of the simplified treatment of drag forces for non-spherical droplets. By dynamically relating the breakup frequency, the pdf of daughter droplets, the critical diameter and the expected life of the particles to the local Weber number, the model is considered suitable for use in the simulation of more complex geometries and cases, such as swirling stabilised burners of typical aeronautical turbine configuration; preliminary results[41] are encouraging.

ACKNOWLEDGEMENTS

This work received funding from the European Community through the project TIMECOP-AE (Project No. AST5-CT-2006-030828). It reflects only the authors' views and the Community is not liable for any use that may be made of the information contained therein.

REFERENCES

[1]Arthur H. Lefebvre, *Atomization and Sprays* (Hemisphere Publishing Corporation, 1989).

[2]F. A. Williams, "Spray combustion and atomization," Phys. Fluids **1**, 541–545 (1958).

[3]John K. Dukowicz, "A particle-fluid numerical model for liquid sprays," J. Comp. Phys. **35**, 229–253 (1978).

[4]M. Pilch and C. Erdman, "Use of breakup time data and velocity history data to predict the maximum size of stable fragments for acceleration-induced breakup of a liquid drop," Int. J. Multiphase Flow **13**, 741–757 (1987).

[5]C. H. Lee and R. D. Reitz, "An experimental study of the effect of gas density on the distortion and breakup mechanism of drops in high speed gas stream," Int. J. Multiphase Flow **26**, 229–244 (2000).

[6]A. Wierzba, "Deformation and breakup of liquid drops in a gas stream at nearly critical Weber numbers," Experiments in Fluids **9**, 59–64 (1990).

[7]Z. Liu and R. D. Reitz, "An analysis of the distortion and breakup mechanisms of high speed liquid drops," Int. J. Multiphase Flow **23(4)**, 631–650 (1997).

[8]L.P. Hsiang and G.M.Faeth, "Near-limit drop deformation and secondary breakup," Int. J. Multiphase Flow **18(5)**, 635–652 (1992).

[9]R. D. Reitz, "Modeling atomization processes in high-pressure vaporizing sprays," Atomization and Spray Tech **3**, 309–337 (1987).

[10]R.D. Reitz and F.V.Bracco, "Mechanism of atomization of a liquid jet," Phys. Fluids **25**, 1730–1742 (1982).

[11]A. D. Gosman and D. Clerides, "Diesel spray modelling: A review," in *Proceedings of the International Conference on Liquid Atomization and Spray Systems-ILASS Europe* (1998) Florence, Italy.

[12]E. Babinsky and P.E. Sojka, "Modeling drop size distributions," Prog. Energy Combust. Sci. **28**, 303–329 (2002).

[13]Viriato Semio, Pedro Andrade, and Maria de Graca Carvalho, "Spray characterization: numerical prediction of sauter mean diameter and droplet size distribution," Fuel **75(15)**, 1707–1714 (1996).

[14]C. Mart'inez-Baz'an, J.L. Montanes, and J.C. Lasheras, "On the break-up of an air bubble injected into fully developed turbulent flow. Part I:Breakup frequency," J.Fluid Mech. **401**, 157–182 (1999).

[15]C. Mart'inez-Baz'an, J.L. Montanes, and J.C. Lasheras, "On the break-up of an air bubble injected into fully developed turbulent flow. Part II:Size pdf of the resulting daughter bubbles," J.Fluid Mech. **401**, 183–207 (1999).

[16]J.C. Lasheras, C. Eastwood, C. C. Mart'inez-Baz'an, and J.L. Montanes, "A review of statistical models for the break-up of an immiscible fluid immersed into a fully developed

turbulent flow," Int. J. Multiphase Flow **28**, 247–278 (2002).

[17]S.V. Apte, M. A. Gorokhovski, and P. Moin, "LES of atomizing spray with stochastic modeling of secondary breakup," Int. J. Multiphase Flow **29**, 1503–1522 (2003).

[18]M. A. Gorokhovski and V. L. Saveliev, "Analyses of Kolmogorov's model of breakup and its application into Lagrangian computation of liquid sprays under air-blast atomization," Phys. Fluids **15(1)**, 184–192 (2002).

[19]Hai-Feng Liu, Xin Gong, Wei-Feng Li, Fu-Chen Wang, and Zun-Hong Yu, "Prediction of droplet size distribution in sprays of prefilming air-blast atomizers," Chem. Eng. Sci. **61**, 1741–1747 (2006).

[20]H. Hiroyasu and T. Kadota, "Fuel droplet size distribution in diesel combustion chamber," Tech. Rep. (University of Hiroshima, 1976).

[21]Sung Wook Park, Sayop Kim, and Chang Sik Lee, "Breakup and atomization characteristics of mono-dispersed diesel droplets in a cross-flow air stream," Int. J. Multiphase Flow **32**, 807–822 (2006).

[22]M. Germano, U. Piomelli, P. Moin, and W. H. Cabot, "A dynamic subgrid-scale eddy viscosity model," Phys. Fluids A **3**, 1760–1765 (1991).

[23]J. Smagorinsky, "General circulation experiments with the primitive equations. I. The Basic Experiment," Monthly Weather Review **91**, 99–164 (1963).

[24]M. Germano, "Turbulence: The filtering approach," J Fluid Mech. **238**, 325–336 (1992).

[25]U. Piomelli and J. Liu, "Large Eddy Simulation of rotating channel flows using a localized dynamic model," Physics of Fluids **7(4)**, 893–848 (1995).

[26]M. Bini and W. P. Jones, "Large eddy simulation of particle laden turbulent flows," J Fluid Mech. **614**, 207–252 (2008).

[27]C. W. Gardiner, *Handbook of Stochastic Methods. For Physics, Chemistry and the Natural Science* (Springer, 1983).

[28]M. Bini and W. P. Jones, "Large eddy simulation of an evaporating acetone spray," Int. J. Heat Fluid Flow **30**, 471–480 (2009).

[29]W. P. Jones, S. Lyra, and A. J. Marquis, "Large eddy simulation of evaporating kerosene and acetone sprays," Int. J. Heat Mass Trans. **53**, 2491–2505 (2010).

[30]M. Bini and W. P. Jones, "Particle acceleration in turbulent flows: A class of nonlinear stochastic models for intermittency.." Phys. Fluids **19**, 035104 (2007).

[31]M. C. Yuen and L. W. Chen, "On drag of evaporating liquid droplets," Comb. Sci. & Tech. **14**, 147–154 (1976).

[32]B. P. Volgin and F. S. Yugai, "Experimental determination of the drag coefficient of a liquid droplet in the process of deformation and breakup in a turbulent gas flow," J. Applied Mechanics and Technical Physics **9**, 118–120 (1968).

[33]E. V. Stekol'shchikov, M. P. Anisimova, I. A. Yatcheni, and O. L. Kondrat'ev, "Experimental study concerning the motion and fragmentation of liquid droplets in a gas stream," J. Engineering Physics and Thermophysics **23**, 957–962 (1972).

[34]M. Bini, *Large eddy simulation of particle and droplet laden flows with stochastic modelling of subfilter scales*, Ph.D. thesis, Imperial College London (2007).

[35]B. T. Helenbrook and C. F. Edwards, "Quasi-steady deformation and drag of uncontaminated liquid drops," Int. J. MultiPhase Flow **28**, 1631–1657 (2002).

[36]Doraiswami Ramkrishna, *Population Balances* (Academic Press, 2000).

[37]C.A. Coulaloglou and L.L.Tavlarides, "Description of interaction processes in agitated liquid-liquid dispersions," J.Fluid Mech. **401**, 183–207 (1999).

[38]S. Rigopoulos, "Population balance modelling of polydispersed particles in reactive flows," Prog. Energy Combust. Sci. **36**, 412–443 (2010).

[39]P. J. O'Rourke and A. A. Amsden, "The TAB method for numerical calculations of spray droplet breakup," SAE Technical Paper 87-2089 (1987).

[40]G. M. Faeth, L. P. Hsiang, and P. K. Wu, "Structure and breakup properties of sprays," Int. J. Multiphase Flow **21**, 99–127 (1995).

[41]W. P. Jones, C. A. Lettieri, J. Marquis, and S. Navarro-Martinez, "Large eddy simulation of the two-phase flow in an experimental swirl-stabilized burner," (2010) Marseille, France.